Electronic Supplementary Information

Growth of $MoSe_2$ nanosheet arrays with small size and expanded spaces of (002) plane on the surfaces of porous N-doped carbon nanotubes for hydrogen production

Bin Qu,[ab] Chunyan Li,[a] Chunling Zhu,[c] Shuo Wang,[a] Xitian Zhang[b] and Yujin Chen*[a]

[a] *Key Laboratory of In-Fiber Integrated Optics, Ministry of Education, and College of Science, Harbin Engineering University , Harbin 150001, China*

[b]*Department of Applied Chemistry, College of Science, Northeast Agricultural University, Harbin 150030, China*

[c]*College of Materials Science and Chemical Engineering, Harbin Engineering University, Harbin 150001, China.*

*Corresponding authors.

Tel.: +086-0451-82519754, Fax: +086-0451-82519754

E-mail addresses: chenyujin@hrbeu.edu.cn (Y. Chen).

Experimental details

1.1 Chemicals. Multi-walled carbon nanotubes with a diameter of 20-40 nm and a length of >5 μm were purchased from Shenzhen Nanotech Port Co., Ltd.. Other regants were purchaged without further treatment.

1.2 Synthesis of the catalysts.

Synthesis of MoO_3/PANI nanohybrids. 0.15 g of α–MoO_3 nanorods was dispersed in 100 mL of 1.0 mol L^{-1} HCl solution by sonication treatment and then the mixture was cooled down to 0°C under stirring (Suspension A). 0.2 mL of aniline was dissolved in 100 mL of 1.0 mol L^{-1} HCl solution, and then transferred to the solution of ammonium persulfate (APS, 0.25 g) dissolved in 100 mL of 1.0 mol L^{-1} HCl solution in the beaker. The mixture solution above was cooled down to 0°C, then transferred to the Suspension A and kept at the temperature for 4 h under stirring. The precipitate was washed by distilled water and ethanol, and then dried at 40°C for 24 h.

Synthesis of $MoSe_2$/NCNTs. MoO_3/PANI nanohybrids were first annealed at 300°C for 2 h at Ar flow, and then MoO_3/MoO_2PANI were obtained. 120 mg of selenium powder was disolved in 20 mL hydrazine hydrate solution, and then 55 mg of MoO_3/MoO_2/PANI powder, 10 mL distilled water and 15 mL ethanol were added under stirring. The mixture was transferred to a Teflon-lined stainless steel autoclave with a capacity of 50 mL for hydrothermal treatment at 220°C temperature for 48 h. The autoclave was cooled down to room temperature naturally, and then the precipitates were washed in distilled water and absolute ethanol under ultrasonication for 10 min, respectively, and dried in a vacuum oven at 60°C. Finally, the dried powder was annealed at 600°C for 2 h under an Ar flow. The sample was named as $MoSe_2$/NCNTs.

Synthesis of $MoSe_2$ spheres. 30 mg of selenium powder was disolved in 5 ml hydrazine hydrate solution, and then 30 mg of MoO_3 powder, 10 mL distilled water and 15 mL ethanol were added under stirring.And then the mixture was transferred to a Teflon-lined stainless steel autoclave with a capacity of 40 mL for hydrothermal treatment at 220°C temperature for 9 h. The resulting precipitate was collected and

washed by deionized water and ethanol, dried at 40 °C for 24 h. Aafter that the dried powder was annealed at 600 °C for 2 h under an Ar flow. The sample was named as $MoSe_2$ spheres.

Synthesis of NCNTs. $MoSe_2$/NCNTs were treated in H_2O_2 solution at 90 °C for 1 h. The resulting precipitate was collected and washed by deionized water and ethanol, dried at 40 °C for 24 h.

1.3 Structure characterization

The morphology and size of samples were characterized by scanning electron microscope (Hitachi SU70) and an FEI Tecnai-F20 transmission electron microscope equipped with a Gatan imaging filter (GIF). X-ray photoelectron spectroscopy (XPS) was carried out by using a spectrometer with Mg Kα radiation (PHI 5700 ESCA System). The binding energy was calibrated with the C 1s position of contaminant carbon in the vacuum chamber of the XPS instrument (284.6 eV). The pore diameter distribution and surface area were tested by nitrogen adsorption/desorption analysis (TRIS-TAR II3020). ICP mass spectrometry was carried out by using a Thermo iCAP 6000 ICP-MS.

1.4 Electrochemical measurements. Electrochemical measurements were performed in a three-electrode system at an electrochemical station (CHI660D). The three-electrode configuration was adopted for polarization and electrolysis measurements, where an Ag/AgCl (KCl saturated) electrode, a graphite rod and $MoSe_2$-based catalysts were used as the reference electrode, the counter electrode and the working electrode respectively. Linear sweep voltammetry with scan rate of 5 mV s^{-1} was conducted in 0.5 M H_2SO_4. For a Tafel plot, the linear portion is fit to the Tafel equation. All data has been corrected for a small ohmic drop based on impedance spectroscopy. All the potentials were calibrated to a reversible hydrogen electrode (RHE).

Glassy carbon disk electrode: 2 mg of catalyst powder was dispersed in 0.5 mL of 3:1 (volume:volume) water/ethanol mixed solvents along with 20 μL of a Nafion solution, and the mixture was sonicated for 30 min. Then, 2.7 μL of the above solution was dropcast onto the surface of a glassy carbon disk electrode at a catalyst loading of around 0.15 mg cm^{-2}. The as-prepared catalyst film was dried at room temperature .

1.5 The TOF calculation. The number of active sites (*n*) was first examined employing cyclic voltammograms with phosphate buffer (pH = 7) at a scan rate of 50

mV s^{-1}. Then the number of the voltammetric charges (Q) could be determined after deduction of the blank value. n (mol) could be determined with the following equation,

n (mol) = Q /2F (HER),

where F is Faraday constant. TOF (s^{-1}) could be calculated with the following equation

TOF (s^{-1}) = I /2nF (HER),

where I (A) was the current of the polarization curve obtained by LSV measurements.

1.6 Identification of the produced gas and determination of FE efficiency. GC measurements were conducted on GC–2014C (Shimadzu Co.) with thermal conductivity detector and nitrogen carrier gas. Pressure data during electrolysis were recorded using a CEM DT-8890 Differential Air Pressure Gauge Manometer Data Logger Meter Tester with a sampling interval of 1 point per second.

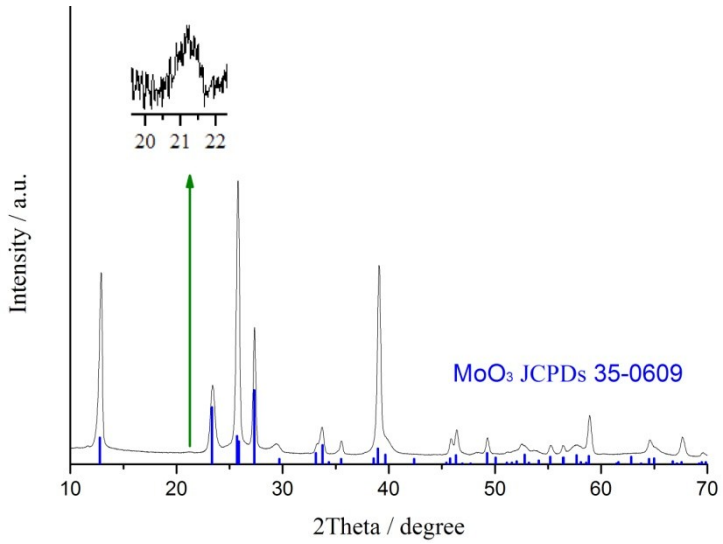

Figure S1 XRD pattern of MoO_3/PANI nanohybrids. Upper inset shows a magnified pattern in the 2theta ranging from 19.5 to 22.2 degree.

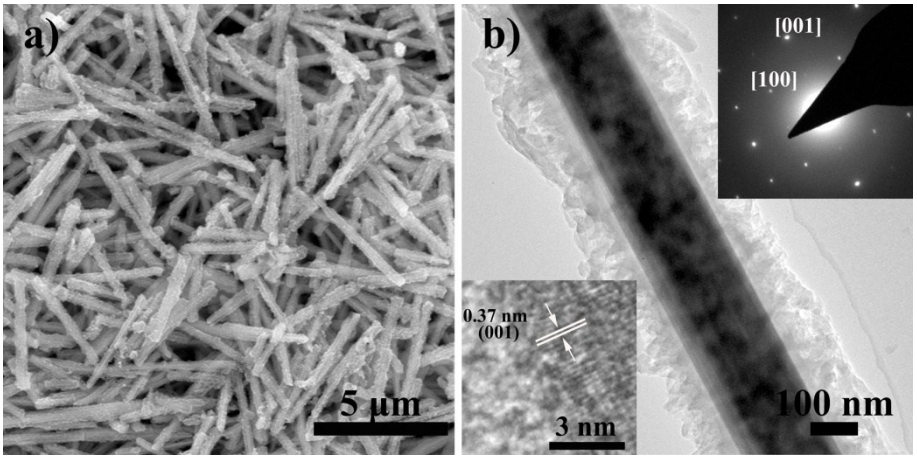

Figure S2 a) SEM and b) TEM image of MoO_3/PANI nanohybrids. Upper inset shows the SAED pattern and bottom inset shows the HRTEM image.

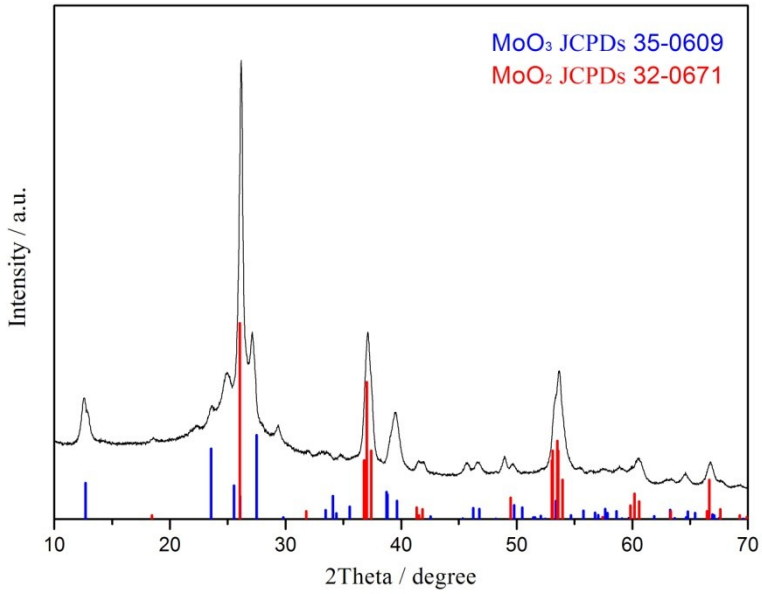

Figure S3 XRD pattern of MoO_2-MoO_3 NCNTs

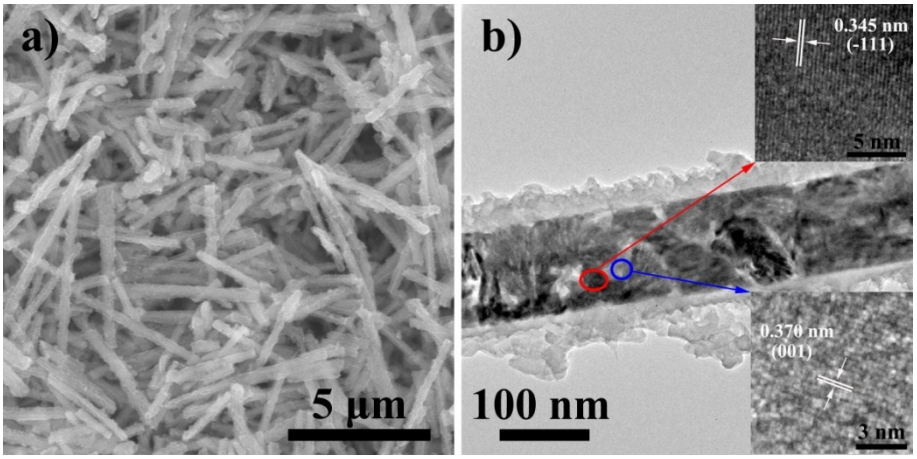

Figure S4 a) SEM image and b) TEM image of MoO_2-MoO_3 NCNTs. The upper and bottom insets show HRTEM images for the dark and grey regions in the middle part of MoO_2-MoO_3 NCNTs.

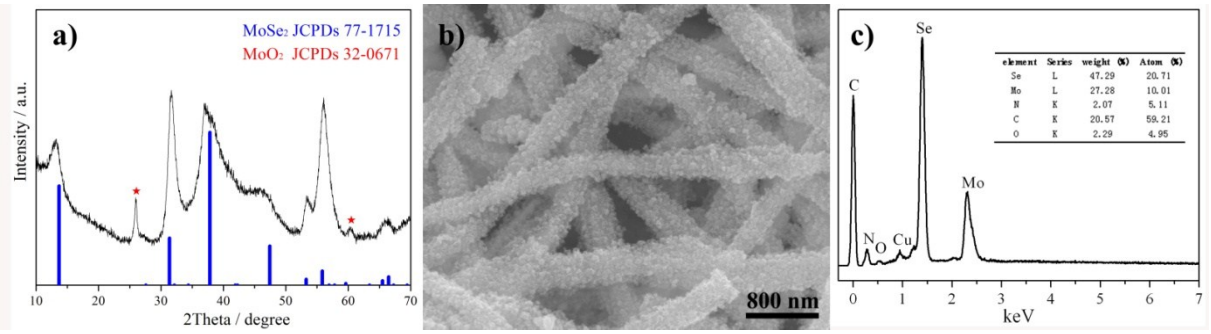

Figure S5 a) XRD pattern of $MoSe_2$/NCNTs , b) SEM of $MoSe_2$/NCNTs, and c) EDS pattern of MoSe2/NCNTs. The inset in c) shows the content of different elements.

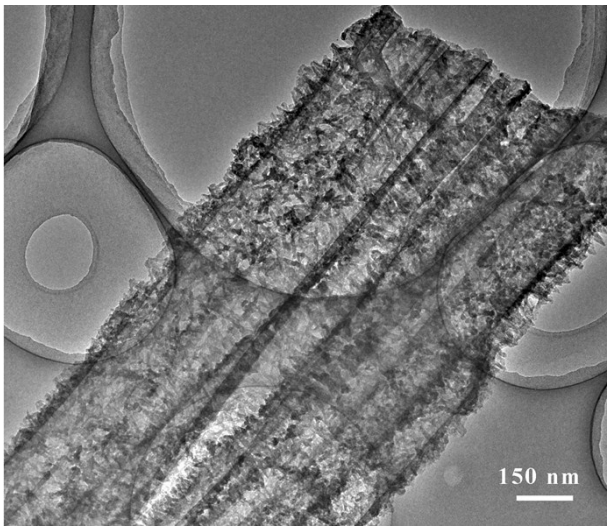

Figure S6 TEM image of NCNTs

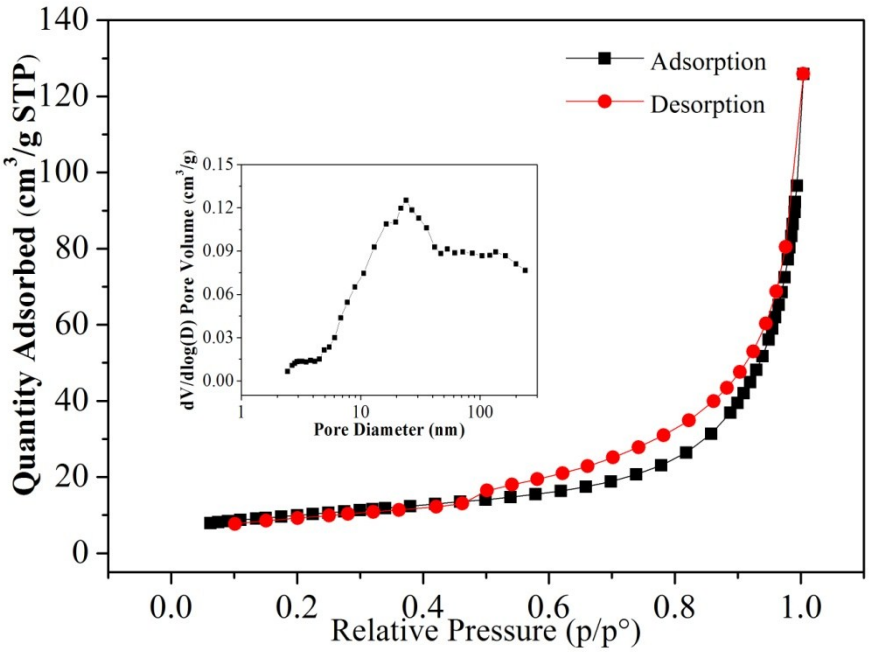

Figure S7 Nitrogen adsorption/desorption isotherms of $MoSe_2$/NCNTs and the inset shows the pore size distribution.

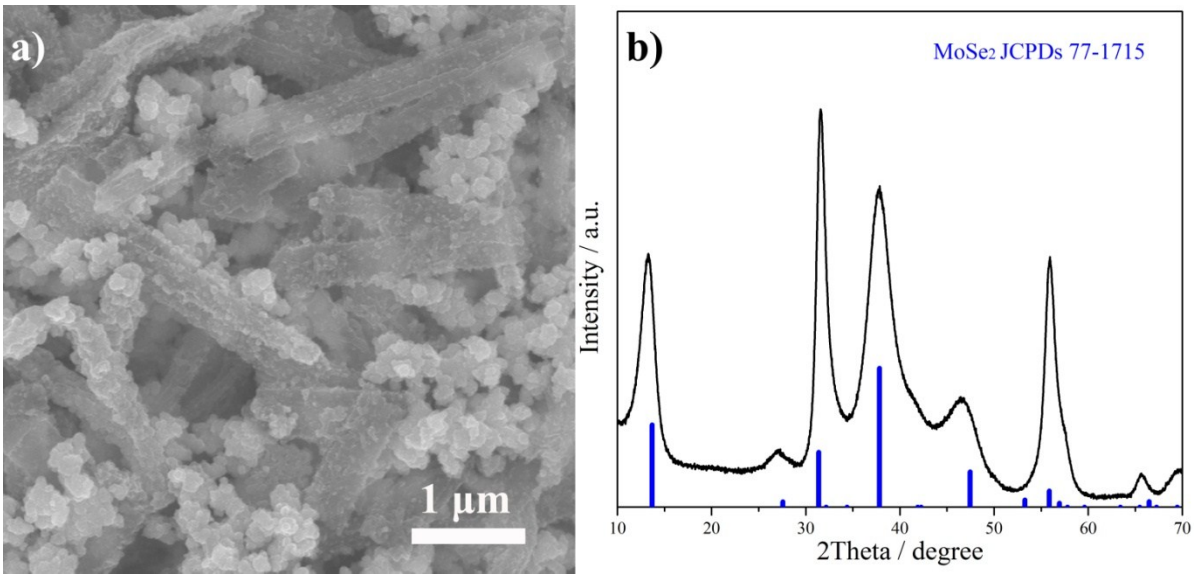

Figure S8 a) SEM of s-$MoSe_2$/NCNTs, b) XRD pattern of s-$MoSe_2$/NCNTs .

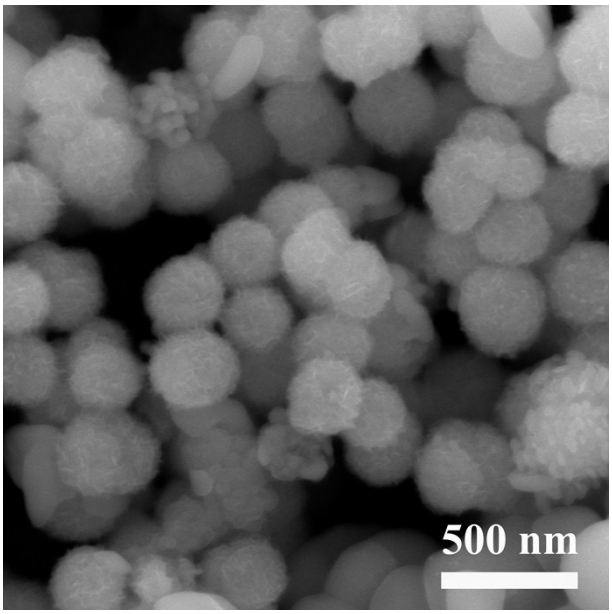

Figure S9 SEM images of $MoSe_2$ spheres.

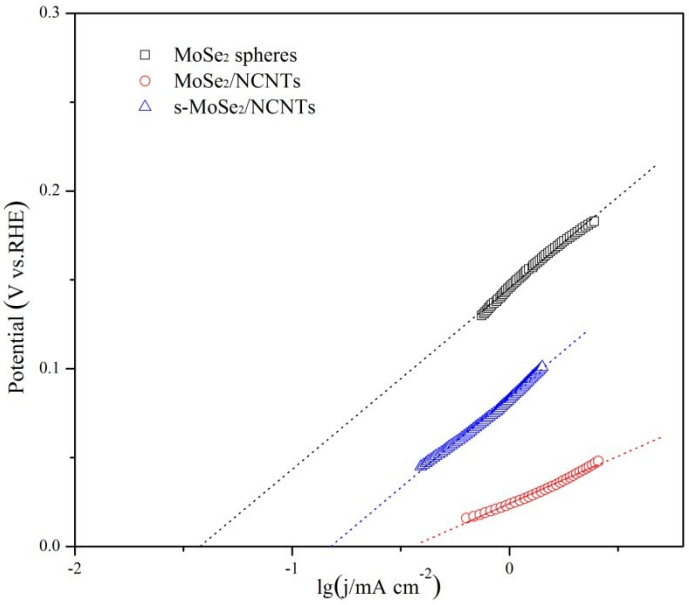

Figure S10 Exchange current densities for $MoSe_2$/NCNT, s-$MoSe_2$/NCNT, $MoSe_2$ spheres extracted from Tafel plots.

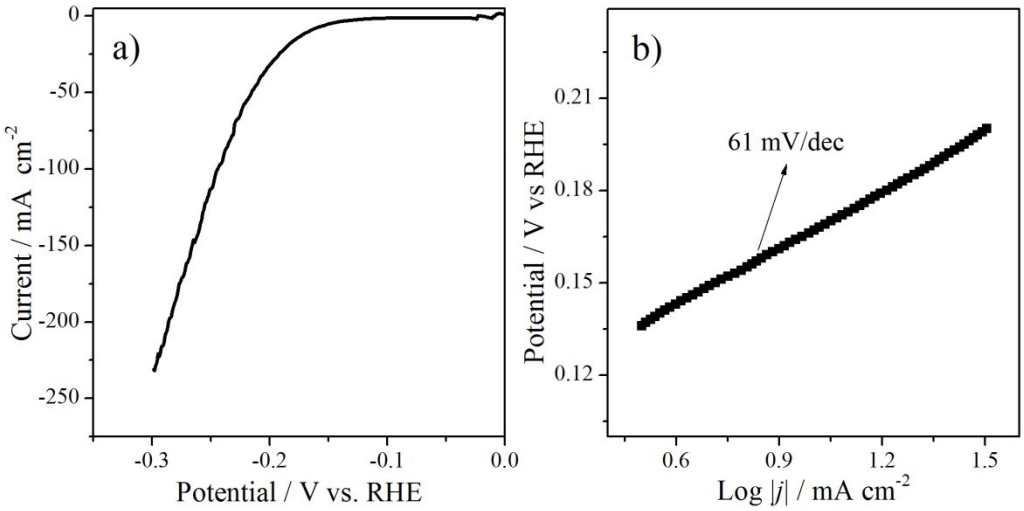

Figure S11 a) The polarization curve of $MoSe_2$/NCNTs loaded on glassy carbon disk electrode toward HER in 0.5 M H_2SO_4 with a scan rate of 5 mV s^{-1}, b) Tafel plots of $MoSe_2$/NCNTs loaded on glassy carbon.

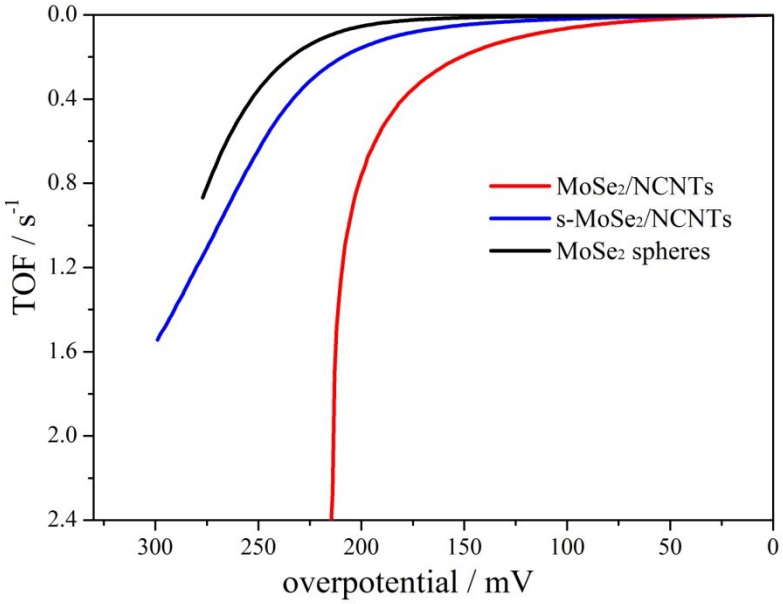

Figure S12 Calculated TOFs for the $MoSe_2$-based electrode films at pH=0 for HER

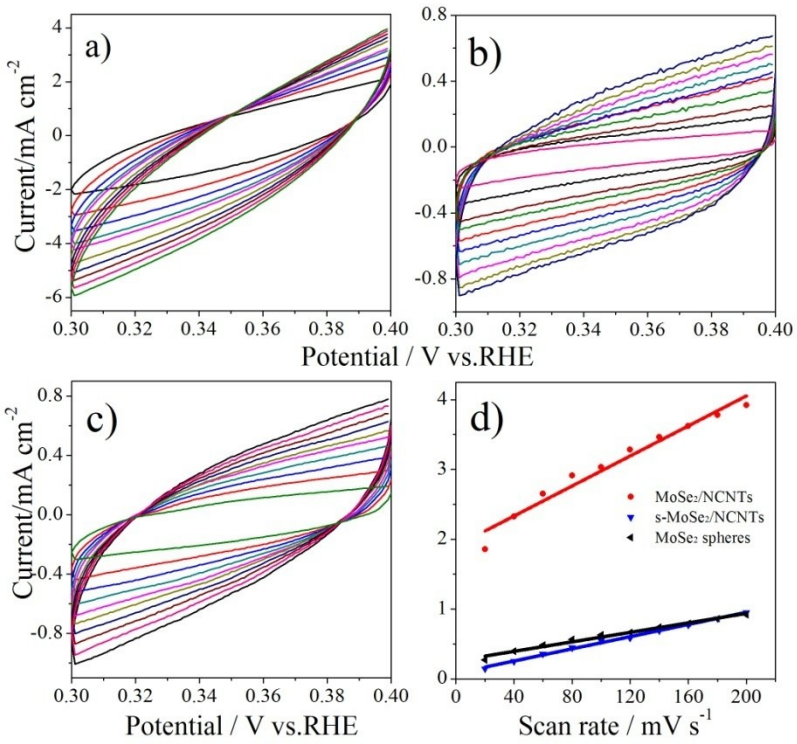

Figure S13 Cyclic voltammograms in the region of 0.3–0.4 V vs. RHE for a) $MoSe_2$/NCNTs, b) s-$MoSe_2$/NCNTs, c) $MoSe_2$ spheres and d) The differences in current density ($\Delta J = J_a - J_c$) at 0.35 V vs. RHE plotted against scan rate fitted to a linear regression allows for the estimation of C_{dl}.

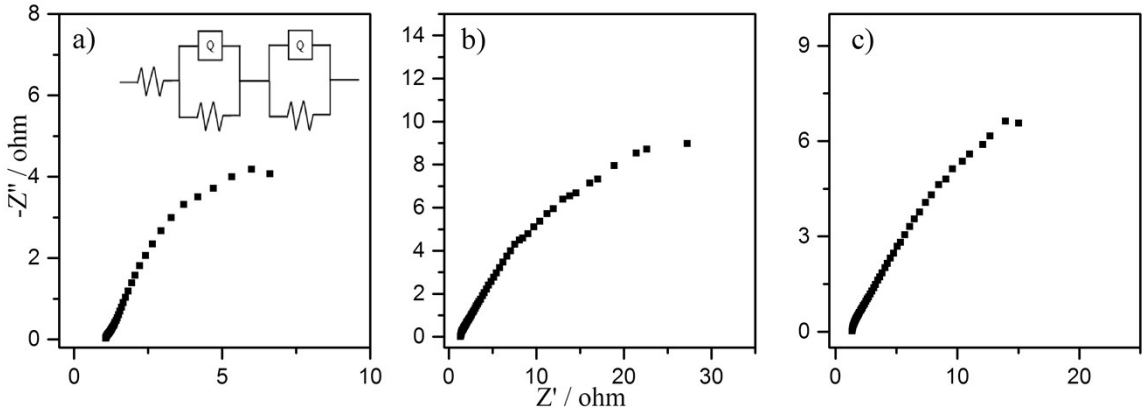

Figure S14 Nyquist plots for a) $MoSe_2$/NCNTs, b) $MoSe_2$ spheres, c) s-$MoSe_2$/NCNTs at an overpotential of 150 mV.

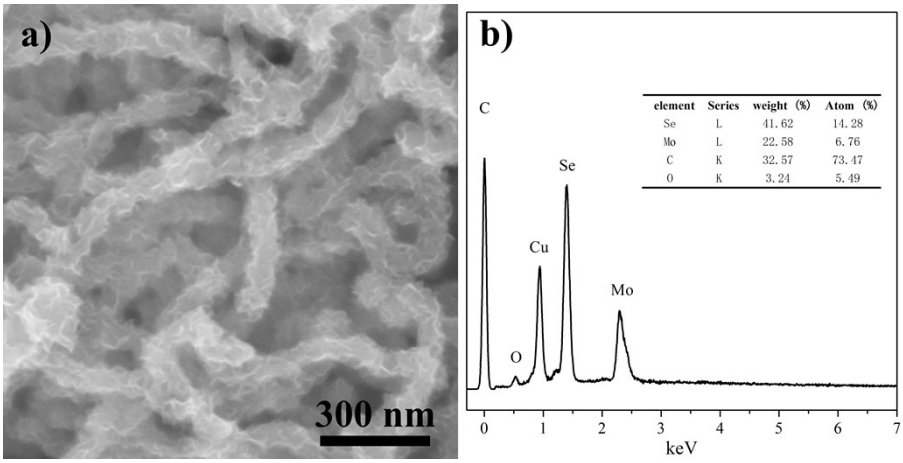

Figure S 15 a) SEM image and b) EDS pattern of $MoSe_2$/CNTs.

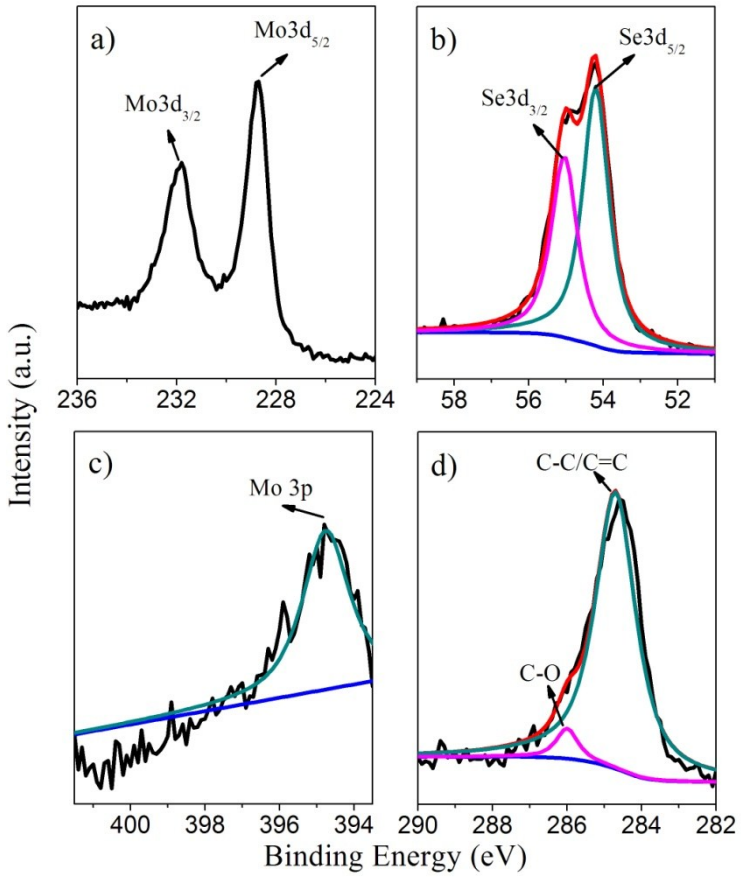

Figure S 16 XPS spectra of $MoSe_2$/CNTs. a) Mo 3d, b) Se 3d, c) N 1s and d) C 1s.

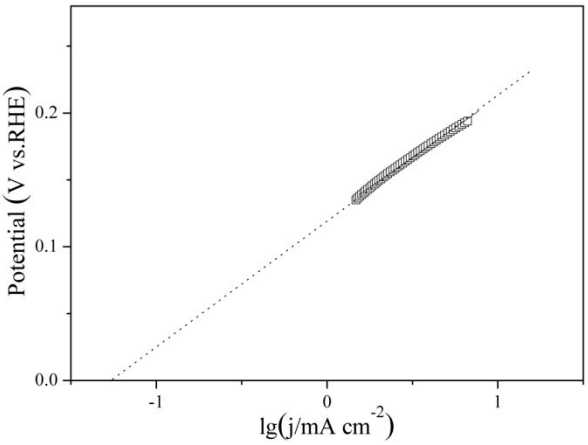

Figure S17 Exchange current density for $MoSe_2$/CNTs.

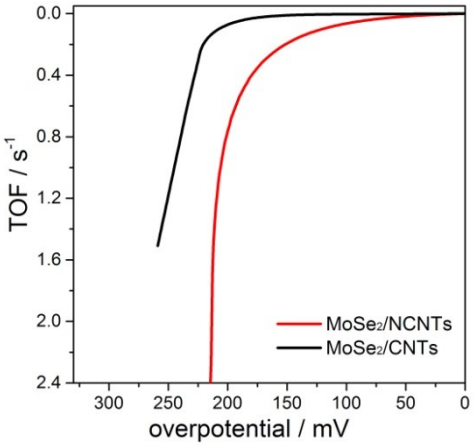

Figure S18 Comparison of TOFs between $MoSe_2$/NCNTs and $MoSe_2$/CNTs.

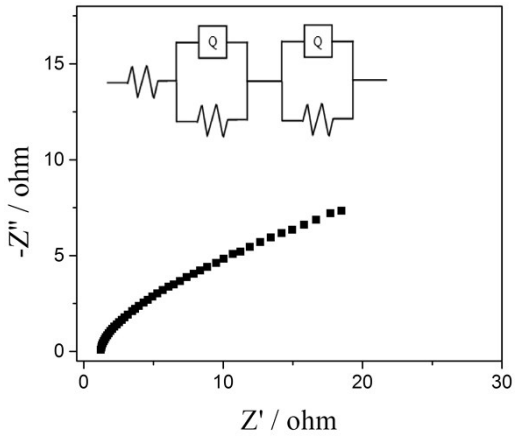

Figure S19 Nyquist plots for $MoSe_2$/CNTs at an overpotential of 150 mV.

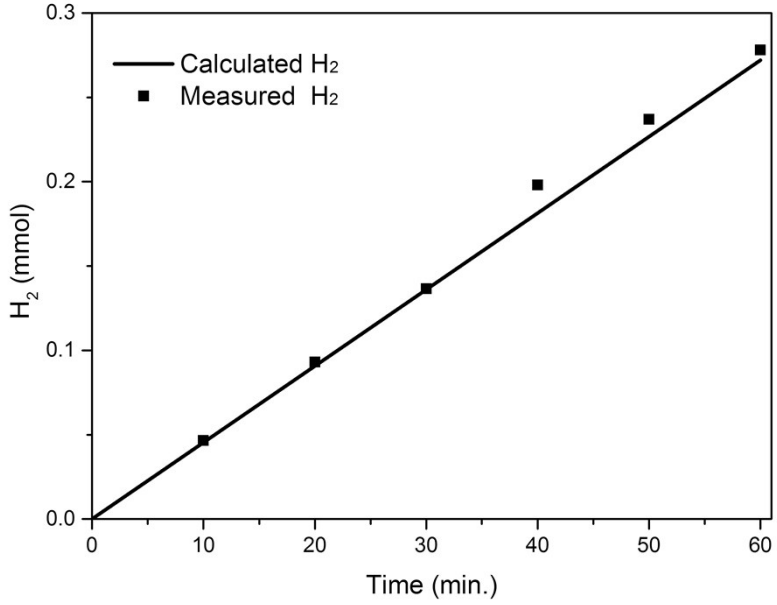

Figure S20 The amount of theoretically calculated (solid line) and experimentally measured (squares) hydrogen versus time for $MoSe_2$/NCNTs at –0.15 V for 60 min.

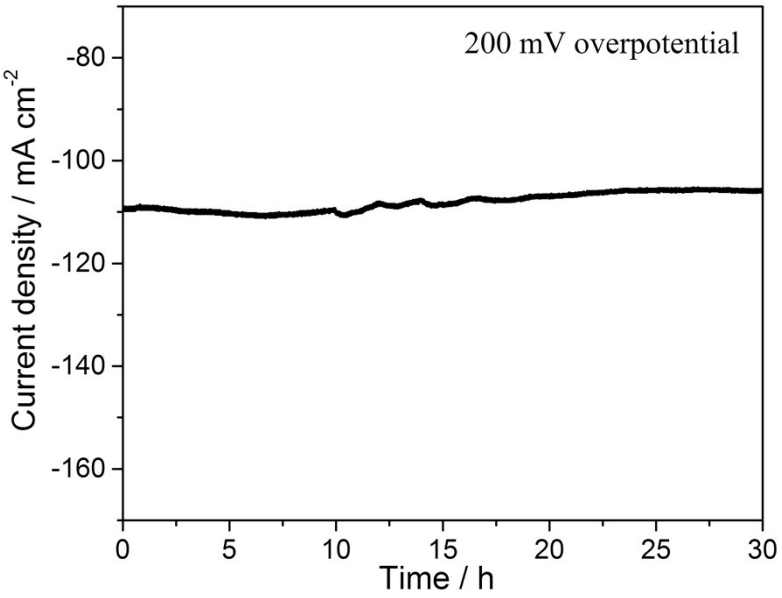

Figure S21 Current stability of $MoSe_2$/NCNTs at a given overpotential of 200 mV.

Table S1. Comparison of HER performance among different $MoSe_2$-based catalysts

Catalyst type	Tafel slope [mV dec^{-1}]	Exchange current j_0 [μA cm^{-2}]	η_{10} (mV)	loading weight (mg cm^{-2})	electrode	Refs
MoS_2/Mo_2C-NCNTs	69	21	—	2	carbon paper	11
MoS_2 nanosheets	55	12.6	—	0.285	glassy carbon	12
$MoSe_2$ thin film	105-120	2.0	—	—	glassy carbon	15
$MoSe_2$ thin film	59.8	0.38	250	—	carbon paper	16
WSe_2 thin film	77.4	—	—	—	carbon paper	16
$MoSe_{2-x}$ nanosheets	98	—	~280	0.285	glassy carbon	17
$MoSe_2$ nanosheets	101	—	290	0.16	glassy carbon	18
$MoSe_2$/RGO hybrid	69	—	115	0.16	glassy carbon	18
CNT@MoSe2	58	—	178	—	glassy carbon	20
SnO2@MoSe2	51	—	174	—	glassy carbon	21
Porous $MoSe_2$ nanosheets	80	—	150	~0.46	glassy carbon	22
$MoSe_2/CoSe_2$	73	117.5	—	0.285	glassy carbon	23
MoSe2/rGO	67	—	195	0.285	rotating disk electrode	25
MoSe2/CNFs	107	—	219	—	PAN film	27
$MoSe_2$ Carbon Fiber Cloth	69	21.1	182	1	Carbon Fiber Cloth	28
$MoSe_2$/CFA	62	—	179	~0.3	glassy carbon	29
$MoSe_2$/GN	61	—	159	—	rGO/PI film	30
$MoSe_x$ nanofilms	100	—	170	—	PLD of $MoSe_x$ films	32
$MoSe_2$ spheres	104	40.7	222	2	carbon paper	This work
S-$MoSe_2$/NCNTs	99	153.3	196	2	carbon paper	This work
$MoSe_2$/NCNTs	53	360.1	102	2	carbon paper	This work
$MoSe_2$/CNTs	68	64.5	191	2	carbon paper	This work
$MoSe_2$/NCNTs	61	19	167	0.15	glassy carbon	This work

Table S2. Comparison of R_s and R_{ct} among different $MoSe_2$-based catalysts. Unit: Ω cm^{-2}

Catalysts	R_s	R_{ct}
$MoSe_2$/NCNTs	1.1	10.4
s-$MoSe_2$/NCNTs	1.1	25.1
$MoSe_2$ spheres	1.4	36.9
$MoSe_2$/CNTs	1.1	15.6